International Journal of Impact Engineering 166 (2022) 104236

Contents lists available at ScienceDirect

International Journal of Impact Engineering

journal homepage: www.elsevier.com/locate/ijimpeng

Development of modelling design tool for harpoon for active space debris removal

J.C. Campbell [1,*], K. Hughes [1], R. Vignjevic [1], N. Djordjevic [1], N. Taylor [2], A. Jardine [2]

[1] Centre for Assessment of Structures and Materials under Extreme Conditions, Brunel University London, Uxbridge, Middlesex UB8 3PH. UK
[2] The Cavendish Laboratory, University of Cambridge, CB3 0HE. UK

ARTICLE INFO

Keywords:
Sandwich panel
projectile impact
explicit finite element
ballistic limit
aluminium alloy

ABSTRACT

The level of debris in Earth orbit presents an increasing risk. Active debris removal, involving capture and deorbit of larger items, has been identified as important in controlling future debris population growth. One concept for capturing debris is a harpoon, with low post-penetration residual velocity being a key design requirement. Aluminium sandwich panels are common structural components on typical spacecraft and consequently a probable target structure. An ideal harpooning event is characterised with complete penetration of the sandwich panel and low harpoon residual (post penetration) velocity. This paper presents development of a numerical modelling tool for a harpoon design for active orbital debris removal. The ability to predict the ballistic limit of an aluminium sandwich panel with a honeycomb core representative of a large satellite structural element being the primary requirement for the modelling tool. The modelling approach was validated against the experimental results from normal and oblique impact tests performed for ogive and flat nose projectiles over a velocity range between 50 m/s to 120 m/s. The modelling was based on explicit finite element method, using the commercial LS-DYNA code. An element failure criterion was used to approximate material damage and failure. Sensitivity studies were performed to investigate the influence of model key features on the projectile exit velocity. The features with the strongest influence were the face sheet material model and the projectile-panel friction model. The projectile exist velocities observed in the experiments were used to select the final parameters used. The use of an element deletion criterion that incorporated the influence of stress triaxiality improved the agreement for the plate deformation behaviour between the numerical and experimental results. For the ogive nose projectile, the exit velocity agreed well with the experiments for the range of impact velocities and angles considered. For the flat nose projectile, the model overestimated the exit velocity. In the case of the normal impact this was due to the model's inability to capture the honeycomb crushing ahead of the projectile.

1. Introduction

The level of debris in Earth orbit is now significant and presents an increasing risk to active satellites. As of January 2021, nearly 22,000 objects of approximately 10cm or larger in Earth orbit are officially catalogued by the U.S. Space Surveillance Network [1]. Of these objects approximately 2,000 are catalogued as rocket bodies and over 6,000 as spacecraft, a number that includes both active and retired payloads. A proportion of these larger items are practical to target for individual capture and deorbit missions. Such a mission would involve launch of a satellite to rendezvous with the debris, capture it and then deorbit in a controlled manner, a concept known as active debris removal [2]. Even the removal of a small number of high-risk objects, about 5 per year, could keep the future Low Earth Orbit debris environment stable [2]. Different methods for capturing derelict satellites have been proposed, with one concept based on the use of a harpoon. A challenge for the harpoon concept is ensuring that the harpoon successfully penetrates the outer structure of the satellite, necessary to ensure a strong attachment. However, this must be achieved over a realistic range of impact velocities and with minimal residual velocity so that the harpoon does not cause further damage.

The objective of this work is the development and validation of a modelling tool for harpoon design. The tool must predict the ballistic limit of an aluminium sandwich panel with a honeycomb core, representative of a large satellite structural element. The ballistic limit being the velocity at which a given projectile will fully penetrate a target.

* Corresponding author
E-mail address: james.campbell@brunel.ac.uk (J.C. Campbell).

https://doi.org/10.1016/j.ijimpeng.2022.104236
Received 19 September 2021; Received in revised form 28 March 2022; Accepted 5 April 2022
Available online 7 April 2022

Good knowledge of the ballistic limit, and its sensitivity to variation in impact conditions, is essential for the harpoon capture concept. This numerical modelling method provides a design tool to support specific harpoon designs. Experimental data from a series of tests was used for model validation. The LSDYNA explicit finite element code was used to simulate the impacts.

The perforation process of a sandwich panel includes perforation of both the front and rear face sheets as well as the core material. While generally the core material offers comparatively low resistance to penetration, the interaction between the face sheets and core adds significant complexity to the panel response. In addition, primarily for oblique impacts, the projectile's path can be altered by the impact with the front face sheet.

There is an extensive literature on ballistic limit studies for a wide range of target materials and shapes subject to impact by varying projectiles. A review of ballistic limit studies can be found in De Vuyst et al. [3], where the ballistic limit of an aluminium sheet impacted by cubical projectiles is studied. The modelling approach for the face sheets in this study was informed by this work.

Studies on the impact response of sandwich structures cover a wide range of face sheet materials, including composite and fibre-metal laminate sheets [4], as well as core materials including foam [5] and lattice structures [6]. Concentrating specifically on metallic panels with a honeycomb core, an analytical model for the ballistic limit of aluminium sandwich panels with a honeycomb core subject to normal impact was developed in 2000 by Hoo Fatt and Park [7], based on experiment results published by Goldsmith et al. [8].

More commonly, investigations combine numerical modelling with experimental tests. Kolopp et al. [9,10] investigated the impact resistance of aluminium panels impacted by spherical projectiles, concluding that the skin-core interactions significantly modify the impact behaviour. Spherical projectiles were also used by Sun et al. [11] who performed a combined experimental and numerical study into the ballistic limit of aluminium panels, investigating the influence of face sheet thickness and the thickness and stiffness of the core. The numerical simulations being used to optimise the energy absorption of the panel. More recently Rahimijonoush and Bayat [12] studied titanium sandwich panels subject to normal impact from hemi-spherical nose projectiles with a length:diameter ratio of 2.5:1. The influence of face sheet thickness was investigated by adding a second layer to the front or rear face sheet, doubling its thickness. They conclude that increasing the rear sheet thickness has a greater effect on the ballistic limit than the front sheet thickness.

2. Experiment

A series of experiments were performed to study the penetration of the aluminium sandwich panels by projectiles. Projectile nose shape and angle of impact were varied.

2.1. Experimental Apparatus

All projectiles were machined from mild steel with a diameter of 20mm. Two nose shapes were used: an ogive of sharpness 1.5 and a flat end. The projectile dimensions are shown in fig. 1, all projectiles had mass 150.0 ± 0.5 g.

The panels were an aluminium honeycomb sandwich structure. The panels consist of two 1.27mm thick aluminium 2024-T81 sheets bonded to an aluminium honeycomb core (Hexcel designation 3/16 – 5056 – 0.0015), for a total thickness of 35 mm. 125 mm square coupons of this material were cut for testing. Each coupon was drilled with four 6.5 mm holes in the corners, on a 105 mm pitch. These holes were used to support the panels during testing. The honeycomb cell size is small, 3/16 inch = 4.76 mm, compared to the 20mm projectile diameter. So the relative position of the projectile and cells was not controlled or investigated.

Two designs of sample holder were used, illustrated in fig. 2. One design holding the panel normal to the projectile path and the second design holding the panel at 45° to the projectile path. For both designs M6 steel studding, passing through the drilled holes in the panel, was used to hold the panels to the sample holder. The diameter of the aluminium washers or spacers in direct contact with the panel was 25 mm. The sample holders themselves were mounted on a 90° L-bracket, which was in turn bolted to the steel base of the target chamber. The projectile path passes through the centre of the panel under test.

Projectiles were launched using a light gas gun with a 20 mm bore barrel. The driving gas was argon, giving a range of velocities accessible between 30 and 120 m/s. A Vision Research Phantom v1610 camera was used for high-speed photography, with a frame rate of 77,490 or 78,947 frames per second depending on the field of view. The camera axis was oriented perpendicular to the projectile direction, and aligned with the centre of the rear face of the panel to minimize perspective distortion of forming fragments and the projectile's emergence. The sides of the target chamber were made from transparent polycarbonate to permit photography, with the panel backlit by a diffuse light source. Inspection of the panels after each test indicated that there was very little out of plane deflection, so the component of residual velocity in the out of plane direction was very small and the single camera was suitable for measurement of the residual velocity.

2.2. Experimental results

Eight experiments were carried out for each combination of projectile and incidence, giving a total of 32. For each experiment the impact velocity (V_{in}) and residual velocity (V_{out}) were measured from the high-speed photography. The results for each are shown in table 1. A simple model of ballistic penetration assumes that, for a particular projectile geometry, the energy lost during penetration is independent of the projectile's incident velocity. This constant energy loss fit was

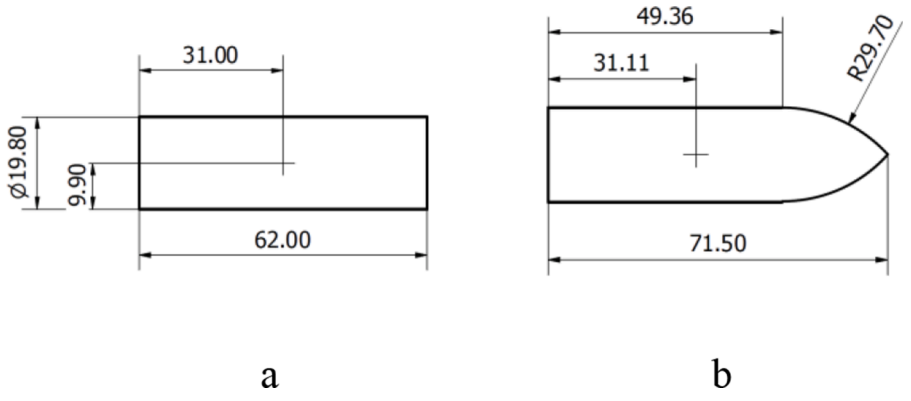

Figure 1. Dimensions in millimetres of flat end (a) and ogive nose (b) projectiles.

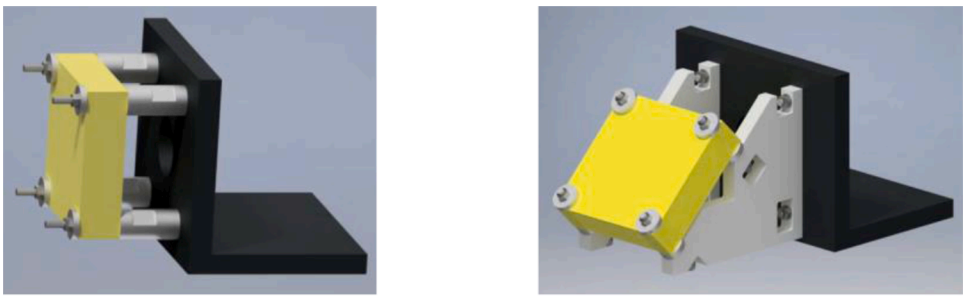

a b

Figure 2. Illustration of panel and sample holder configurations for (a) normal impact and (b) 45° impact. In both cases the projectile approaches from the right, passing through a hole in the dark-grey L-bracket before impacting the panel.

Table 1
Impact velocity and residual velocity measured for each experiment. The energy of penetration for each case is calculated assuming the energy lost is independent of the impact velocity, shown with the 1σ uncertainty. The experiments marked with a * indicate that the result was considered anomalous and not used when determining the penetration energy.

Ogive Nose Normal Incidence			Flat Nose Normal Incidence			Ogive Nose 45° Incidence			Flat Nose 45° Incidence		
Expt.	**V_{in} (m/s)**	**V_{out} (m/s)**	**Expt.**	**V_{in} (m/s)**	**V_{out} (m/s)**	**Expt.**	**V_{in} (m/s)**	**V_{out} (m/s)**	**Expt.**	**V_{in} (m/s)**	**V_{out} (m/s)**
1	97.4	87.7	1	101.9	81.5	1	118.4	104.5	1	122	101.2
8	88.9	77.7	3	90.6	68.4	8	106.9	88.4	8	113.4	92.9
4	71.5	57.4	8	90.0	57.3	7	93.9	79.6	7	100.5	76.7
6	65.0	42.3	4	85.0	50.4	2	80.3	56.7	2	91.3	66.9
2	61.4	41.9	5	81.2	54.6	6	76.8	52.4	5	80.4	56
5	55.8	29.25	6	79.3	45.3	5	74.3	48.2	3	71.1	42.3
3	50.1	15.4	7	74.3	30.8	4*	72.0	52.0	4	60.9	21.3
7	49.2	21.5	2*	73.7	0	3*	59.0	38.3	6	57.5	21.6
Penetration energy: 154±6 J			Penetration energy: 310±16 J			Penetration energy: 233±9 J			Penetration energy: 268±14 J		

determined for each case and is included in table 1. Figure 3 shows the residual velocities and constant energy loss fit curves for all four cases. There were three results considered anomalous in the data, and not used for the constant energy loss fit. In experiment 2 for the flat nose normal incidence case the projectile failed to penetrate, and a subsequent experiment (number 7) at a similar velocity did penetrate with a significant residual velocity. In experiments 3 and 4 for the ogive nose 45° incidence case, the projectile was deflected by the rear sheet and exited through the side of the panel rather than penetrating the rear sheet. This behaviour is discussed in more detail in section 4.2.

3. Numerical Model

A finite element model of the panel was developed for the explicit LSDYNA analysis code. The model development analyses used LSDYNA R8.0 SMP on a 64-bit Windows PC. Later analyses used LS-DYNA R10.1 MPI on a 24 core linux computing node. No significant difference was observed in the results between the two versions.

3.1. Model development

The first stage was to build a development model of the panel that

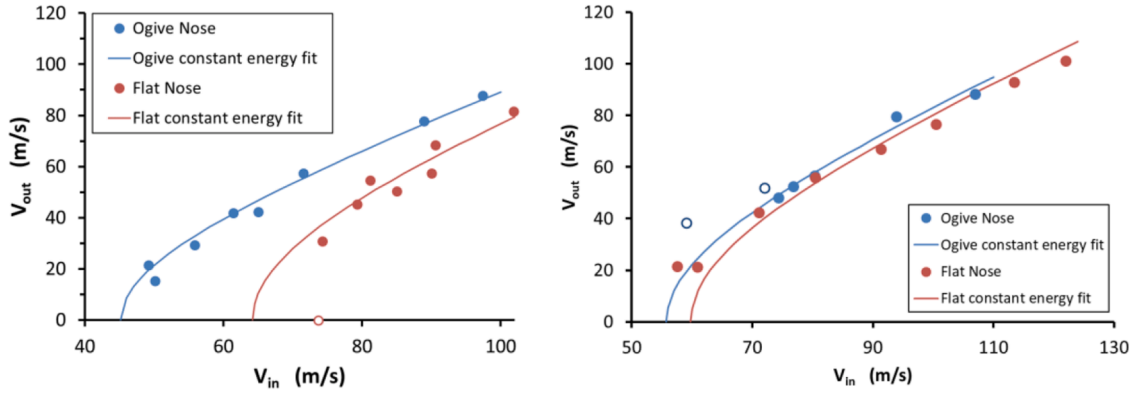

a b

Figure 3. Comparison of residual velocities with varying projectile shape for 20 mm projectiles at (a) normal incidence, and (b) 45° incidence. Hollow data points indicate a result not used when determining the penetration energy.

would be the basis for sensitivity studies to investigate modelling assumptions. Following previous experience with modelling the ballistic limit of aluminium plates [3] a detailed meshing approach was taken, with the face sheet meshed using solid elements. Based on the mesh sensitivity studies conducted for the aluminium plate study [3], five elements through the face sheet thickness was selected for this model. To manage the model computational cost the in-plane element size was increased away from the impact location, resulting in 207,480 hexahedral elements per sheet. Following this detailed approach, the honeycomb core geometry was directly modelled using 378,160 shell elements. The main assumptions present in the development model are: element erosion for the plate and foil material using a plastic strain erosion criterion; a rigid projectile; rigid plate supports.

An impact velocity of 74m/s with a 0° angle with an ogive nose projectile was selected as the reference case for the sensitivity studies. For this velocity a 154 J energy loss would result in an exit velocity of 58.5 m/s.

The second stage in the model development process was to run a series of sensitivity studies to investigate the influence of modelling assumptions on the projectile exit velocity. The parameter with the strongest influence on the projectile exit velocity was the coefficient of friction used for the projectile-panel contact. A value of 0.47, the coefficient of sliding friction for aluminium on mild steel [13], resulted in the projectile failing to fully penetrate the panel. The dynamic friction coefficient for metal-metal interfaces at high impact velocities, significantly above the velocities relevant for harpoon impact, has been shown to be small (≈0.01) [14], establishing a lower limit for the value of the coefficient. In the velocity range relevant for this work the coefficient of sliding friction is influenced by the relative velocity of the two surfaces and the normal pressure in addition to the material and surface finish [15]. For steel-steel contact at a relative velocity ≈ 55 m/s, Phillipon et al. [16] measured a friction coefficient range from 0.31 decreasing to 0.15 as the normal pressure increased. The results from the sensitivity study on the friction coefficient using the development model are shown in table 2. While a friction coefficient of 0.01 gave the best agreement for exit velocity, the review of literature [14–16] suggested this value is low for the actual impact conditions. A coefficient of 0.1 was selected as the highest value consistent with a reasonable exit velocity. This value for the friction coefficient is used for all simulation results shown in this paper.

The other primary outcomes from this stage were:

- The strength and failure strain of the face sheets influenced the exit velocity, though not as strongly as the friction.
- The strength and failure strain of the aluminium foil did not significantly influence the exit velocity.
- The assumption of a rigid projectile is appropriate as no significant deformation of the projectile occurred in the experiment.
- The assumption of rigid supports is not appropriate.
- Failure between the face sheets and honeycomb core should be permitted. This only has a small influence on projectile exit velocity, but does have a visible influence on the level of dishing seen in the rear sheet.

In the final stage an updated reference panel model was developed, this model is presented in detail in the following section.

Table 2
Projectile exit velocities for projectile-panel contact friction coefficient sensitivity study.

Friction Coefficient	Projectile exit velocity (m/s)
0.47	Did not exit
0.2	47.9
0.1	52.4
0.05	55.1
0.01	57.4

3.2. Reference model

The model represents panel and supports as tested, fig. 4. The panel is impacted by a 20mm diameter, 150g, steel projectile with an ogive or flat nose.

3.2.1. Face sheets

The face sheet is meshed from constant stress hexahedral elements, with five elements through the sheet thickness. At the impact location the elements are approximately cubic with an in-plane edge length varying between 0.233 mm and 0.274 mm. The in-plane mesh resolution is reduced away from the impact region, consequently different face sheet meshes are required for the 0° and 45° impact cases, shown in fig. 5 a and b respectively. The mesh at the impact location is the same for both. The total number of elements in each sheet is 251,360 for the 0° case and 249,930 for the 45° case. Different material models were investigated and will be discussed in section 3.3.

3.2.2. Honeycomb core

The honeycomb core was modelled using four elements along each cell edge and forty through the core thickness for a total of 358,176 elements, fig. 6. A bi-linear elastic plastic constitutive model was used. Published data for the strength of 5056 aluminium foil [17] was used to select a yield stress of 435MPa and tangent modulus of 7.5MPa. The honeycomb model was verified by running an unconstrained crush test and comparing against the published crush strength of 2.14 MPa (converted from the value of 310 psi given in the source) [18]. The model gave an average crush stress of 2.03MPa over a displacement of 15mm, ignoring the first 1mm of displacement due to the initial compressive peak.

3.2.3. Projectile and support

Ogive nose and flat nose versions of the projectile were developed, fig. 7. In both cases the projectile diameter is 20mm and the mass is 150g. The projectile is treated as rigid for simplicity as the experimental video showed no visible projectile deformation. The supports at each corner were identical, a detail view of one support is shown in fig. 8. The support base, studding and nut were modelled as low-carbon steel with a yield strength of 317 MPa. The base of the support was fully fixed. The washer interacted with the sandwich panel and support through contact only, it was modelled as aluminium with a yield strength of 277 MPa.

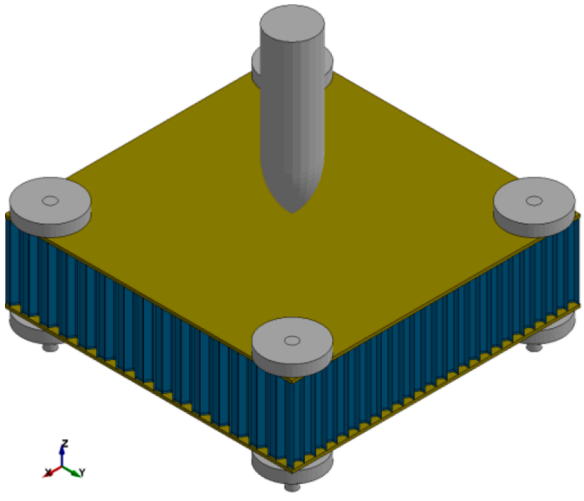

Figure 4. Reference panel model assembly with 0° ogive nose projectile.

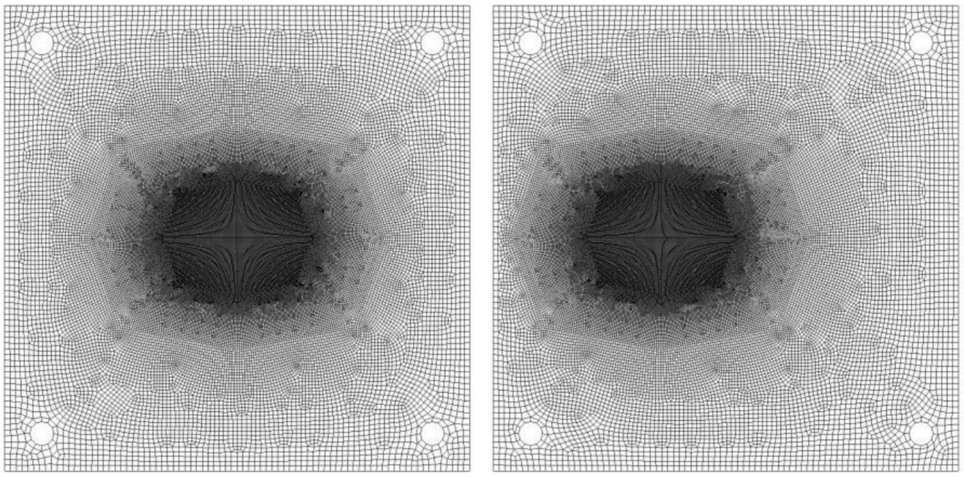

Figure 5. Face sheet mesh. (a) 0° impact case (b) 45° impact case.

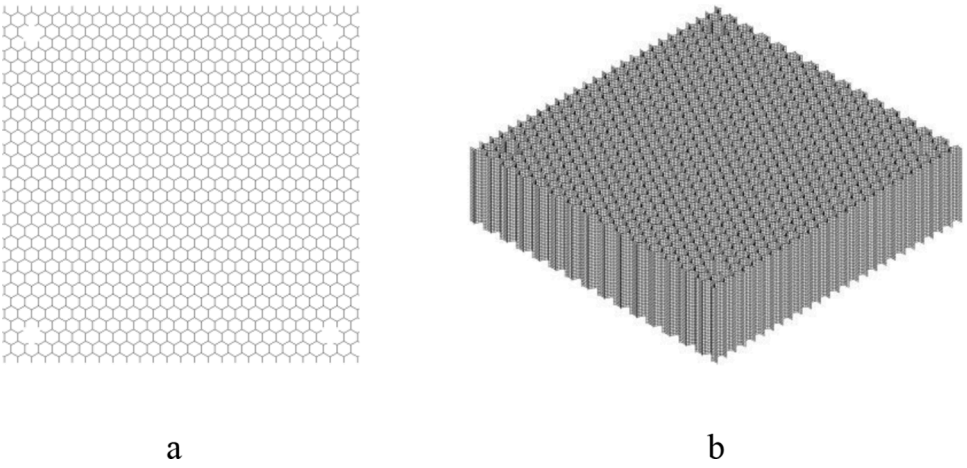

Figure 6. Honeycomb core model. a)top view, b)isometric view.

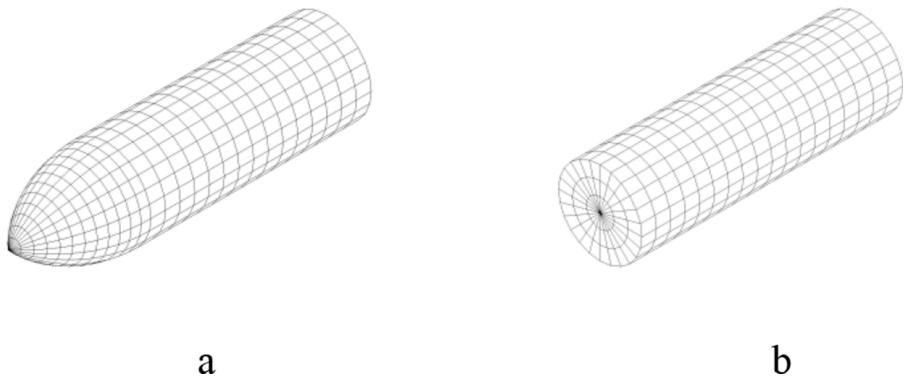

Figure 7. Rigid projectile models. a) Ogive nose b) Flat nose.

3.2.4. Contact

Eroding contact was used between the projectile and panel with a friction coefficient of 0.1. A tiebreak contact was used for the core to face sheet with a normal failure stress of 6 MPa, this value was taken from the LS-DYNA offset deformable barrier models developed by LSTC [19]. No experimental data was available for the specific panels to assess this assumption.

3.3. Al 2024-T81 material modelling

The two face sheets are manufactured from aluminium 2024-T81. The T81 temper is artificially aged, resulting in a higher strength and

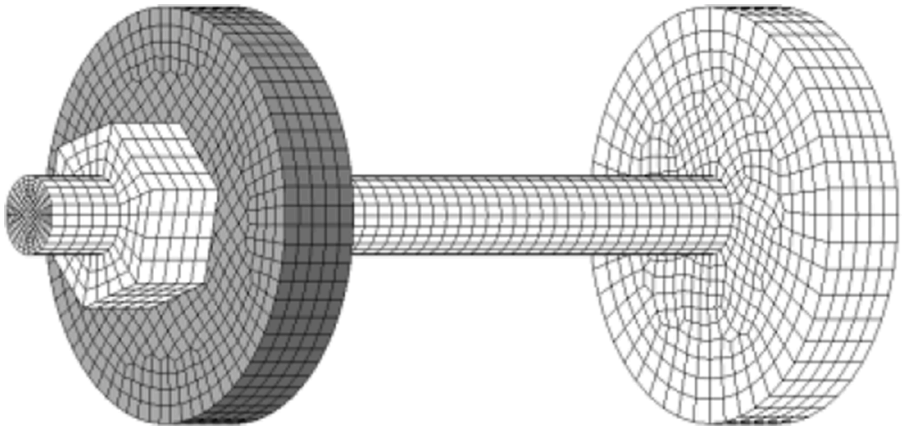

Figure 8. Support model. Aluminium washer (grey) is a separate part, interacting through contact only.

lower ductility than the more commonly used T3 temper. A single untested panel was available for material characterisation and two tension test specimens were cut from this panel. A piecewise linear flow stress vs plastic strain curve was derived from the test data, fig. 9, and included in LSDYNA as material type 24 (*MAT_PIECEWISE_LINEAR_PLASTICTY) [20] with elements deleted using an effective plastic strain to failure value. This curve was verified by modelling the tension tests using the same mesh density as the face sheet, five elements through the thickness, and deriving the resulting stress strain curve from the numerical extensometer and force transducer data, fig. 10.

From the sensitivity study an effective plastic strain to failure of 0.15 was selected for the face sheets, giving a projectile exit velocity of 55.8 m/s. While this is lower than the exit velocity representative of 154J energy loss, a reduced value of erosion strain would increase the exit velocity, it represents a compromise between the exit velocity and tension test model results. Comparing the model results to the experimental high-speed video, fig. 11, showed that the deformation of the rear face sheet in the model was not correct. In the experiment the projectile penetrates the rear face sheet through initial dishing followed by petalling type failure, behaviour consistent for all normal impact experiments with the ogive projectile. By contrast the dishing in the model is significantly less pronounced and the projectile leaves a circular hole in the sheet with most elements deleted in this region. Consequently, alternative material models for the face sheet were investigated to improve the plate deformation behaviour.

The first option investigated was replacement of the plastic strain failure model with a continuum damage mechanics model. The model selected for this was LSDYNA material type 153 (*MAT_DAMAGE_3). This model allows the use of the same flow stress curve and is an implementation of a model developed by Lemaitre [21]. This model

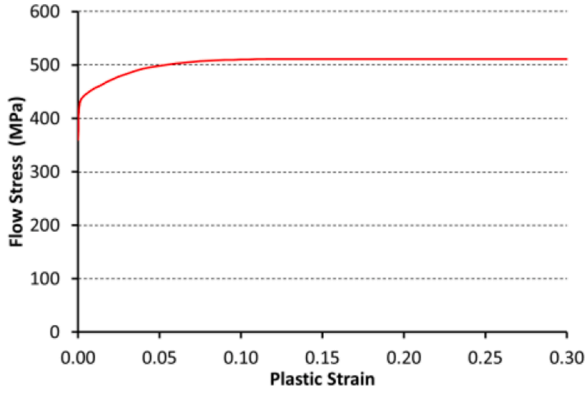

Figure 9. Piecewise liner flow stress vs. plastic strain curve for face sheets derived from tension tests.

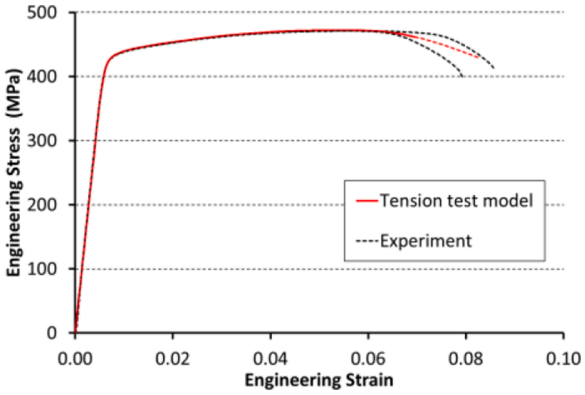

Figure 10. Tension test model results (red line) and experimental results for the two specimens. The solid red line is for plastic failure strain of 0.15, the dashed red line extends this to a failure strain of 0.40.

requires four parameters which were estimated following sensitivity studies with the tension test model as: threshold plastic strain for damage, 0.15; damage material constant S, 1.8 MPa; damage material constant t, 3.0; critical damage for element deletion, 0.5.

Using material type 153 for the face sheets, the projectile exit velocity was 56.2 m/s and visually similar behaviour to the experimental video was seen in the rear sheet, fig. 12. The use of a strain softening material model is well known to introduce mesh dependence, see for example Belytschko et al. [22]. Therefore the mesh sensitivity of this model using material type 153 was checked and found to be significant. Regularization through the use of non-local damage, using the LS-DYNA *MAT_NONLOCAL option, was investigated. While this reduced the mesh dependence, it did not prove possible to develop a robust panel model that reliably ran to projectile exit. As there was also a significant increase in computational cost, it was decided not to use material 153 in this study.

The second option investigated was the use of a more complex element failure model. The Johnson-Cook failure model [23] has been used in a number of published studies on ballistic impact and high-strain rate failure of aluminium [24–30]. This model defines a failure strain that is dependent on the triaxiality, strain rate and temperature.

Material type 224 (*MAT_TABULATED_JOHNSON_COOK) was selected as it allowed the piecewise linear flow stress vs plastic strain curve to be retained. Material type 224 resembles the Johnson-Cook model [31] in that the effects of strain, strain rate and temperature are combined multiplicatively. The use of tabulated rather than analytical input for the specific relationships allowing for a wider range of material behaviour to be represented. In this model the flow stress, σ_y,

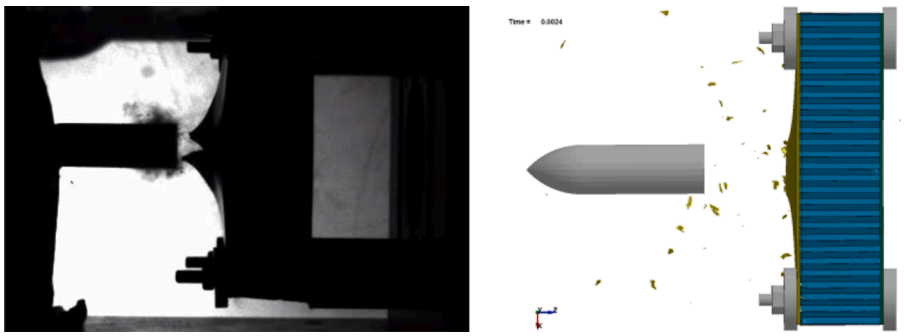

Figure 11. a) Still from high speed video for 71.5 m/s impact velocity showing panel deformation immediately following projectile exit. b) Model result for 74 m/s impact velocity showing panel deformation.

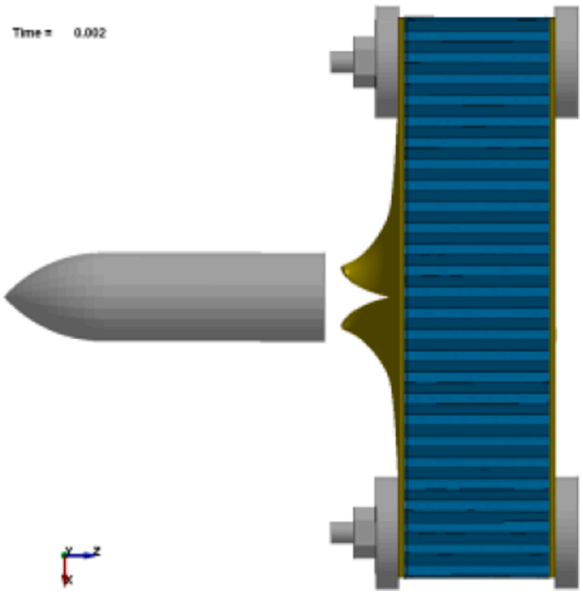

Figure 12. Result for 74 m/s impact with using material type 153 for face sheet.

is defined as a function of plastic strain, ε_p, plastic strain rate, $\dot{\varepsilon}_p$, and temperature, T, as [20]:

$$\sigma_y = k_1\left(\varepsilon_p, \dot{\varepsilon}_p\right)\frac{k_T\left(\varepsilon_p, T\right)}{k_T\left(\varepsilon_p, T_R\right)}.$$

The plastic failure strain, ε_{pf}, is defined as a function of stress triaxiality, Lode parameter, plastic strain rate, temperature and element characteristic length, l_0, as [20]:

$$\varepsilon_{pf} = f\left(\frac{p}{\sigma_{vm}}, \frac{27J_3}{2\sigma_{vm}^2}\right)g\left(\dot{\varepsilon}_p\right)h(T)i(l_0)$$

As the only specific data available for the face sheet material was the quasi-static tension test results shown in fig. 10 and published data on the 2024-T81 temper is limited, for this study it was assumed that 2024-T3 data for effects other than strain hardening could be used instead. The temperature dependence of both the flow stress and failure strain was ignored. The plastic strain rate dependence was assumed to follow the common Johnson-Cook relationships of $(1 + C\ln\dot{\varepsilon}^*)$for the flow stress, and the $(1 + D_4\ln\dot{\varepsilon}^*)$for the plastic failure strain. The tabulated values were determined using $C = 0.0083$ and $D_4 = 0.011$, both values derived for 2024-T3 by Leuser [32].

The dependence of the failure strain of the triaxiality was estimated based on the data for 2024-T351 published by Wierzbicki et al.[33]. A failure strain vs triaxiality scale factor was defined, fig. 13, to scale the

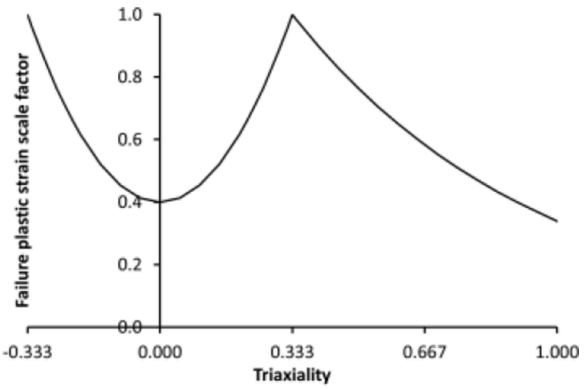

Figure 13. Scale factor for triaxiality dependence of failure strain used for this study.

uniaxial stress failure strain.

A sensitivity study for the reference plastic failure strain was conducted and a value for the effective plastic strain at failure of 0.25 gave a projectile exit velocity of 55.1 m/s. Improved agreement for the visual behaviour of the rear face sheet was also seen, fig. 14.

4. Modelling results

Following the impact cases studied experimentally, chapter 2, four primary impact configurations were studied. These configurations comprised two projectile geometries, ogive nose and flat nose, with a normal impact (0°) and an oblique impact (45°) case for each projectile.

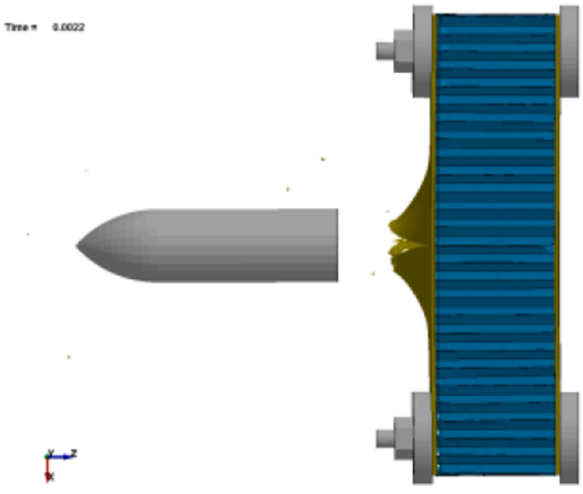

Figure 14. Result for 74 m/s impact with using material type 224 for face sheet

The four initial configurations are shown in fig. 15. For each configuration the model was run at a range of impact velocities to establish the ballistic limit, using both the Piecewise Linear Plasticity (PLP) and Tabulated Johnson Cook (TJC) models established previously for the face sheets. Other than the projectile geometry, orientation and velocity and the material model used for the face sheets, the only other difference in the models used in this section was the face sheet mesh for the normal and oblique impact cases discussed in section 3.2.1.

4.1. Ogive nose normal impact configuration

For this configuration analyses were run for six impact velocities: 44 m/s, 48 m/s, 55 m/s, 60 m/s 74 m/s and 98 m/s. A graph of projectile exit velocity against impact velocity is shown in fig. 16 for both face sheet strength models, along with the experimental results. The 74 m/s impact case is the condition used for the sensitivity study and tuning of model parameters. The results show that the model agrees well with the experimental trend, and predicting a ballistic limit consistent with the experimental data. Further tuning of the PLP or TJC constitutive model parameters, along with the friction model parameters, could lead to improved agreement with the experimental results. As it was not possible within this study to obtain additional experimental characterisation data to support this process, further tuning was not considered appropriate for this study.

4.2. Ogive nose oblique impact configuration

For this configuration analyses were run for seven impact velocities: 55 m/s, 60 m/s, 64 m/s, 74 m/s, 80 m/s, 93 m/s and 103 m/s. These velocities cover the range of impact conditions tested experimentally.

A graph of projectile exit velocity against impact velocity is shown in fig. 17. This shows good agreement between the experimental and numerical results at higher impact velocities above 70m/s, but an increasing overestimate of the energy absorbed at lower velocities. This is significant as a change in behaviour is seen in the experimental results above and below 70 m/s. At the higher velocities the projectile fully penetrates the panel and the numerical behaviour agrees well with the experimental behaviour, fig. 18. At lower velocities the projectile does not fully penetrate the rear sheet, instead it is deflected by the sheet and exits the side of the panel as shown in fig. 19. In fig. 17 the experiments where this occurs are denoted by the outline only data points. While this change in behaviour is also seen in the numerical results, the critical velocity where the change occurs is under estimated. Investigation of the causes behind this change in behaviour showed that in addition to the rear face sheet properties and interaction with the core material the interaction of the projectile with the front face sheet is also critical as this influences the orientation of the projectile when it first contacts the rear sheet.

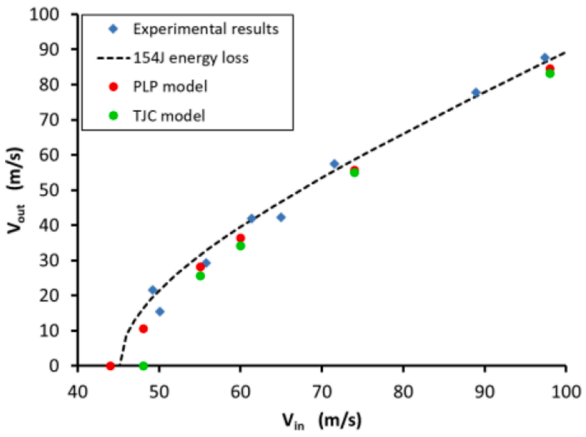

Figure 16. Ogive nose normal impact configuration model results plotted with the experimental results and the 154 J energy loss fit to the experimental data. The graph shows projectile exit velocity, V_{out}, against initial impact velocity, V_{in}.

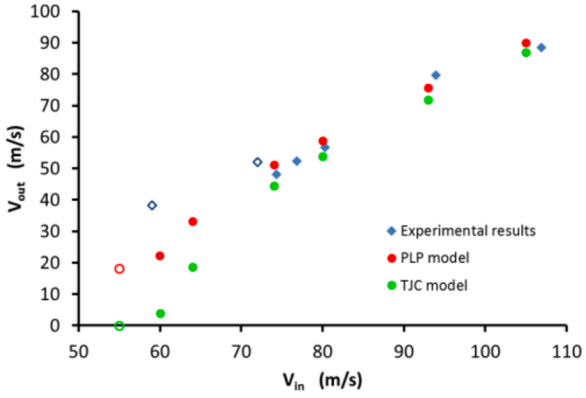

Figure 17. Ogive nose oblique impact configuration model results plotted with the experimental results. The filled symbols represent cases where the projectile penetrates the rear sheet. The outline only symbols represent the cases where the projectile exits the side of the panel.

4.3. Flat nose normal impact configuration

For this configuration analyses were run for five impact velocities: 65 m/s, 74 m/s, 82 m/s, 90 m/s and 105 m/s. These velocities cover the range of impact conditions tested experimentally.

The flat nose of the projectile significantly alters the penetration mechanics. For the front sheet the mode of penetration changes from petalling to plugging. The projectile with plug then travels through the

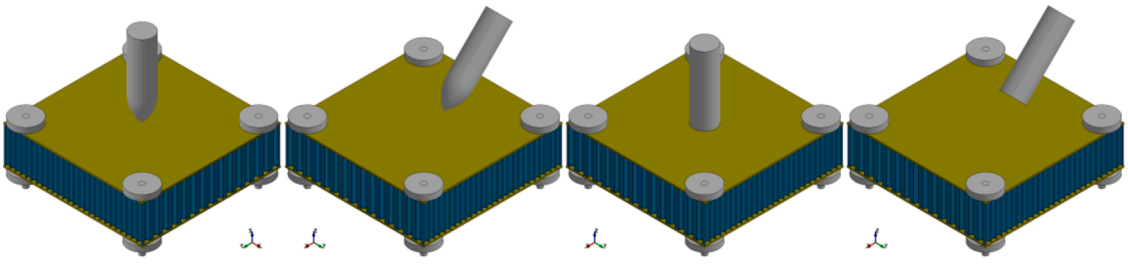

Figure 15. View of initial state for the four configurations investigated: a) ogive nose normal impact b) ogive nose oblique impact c) flat nose normal impact d) flat nose oblique impact

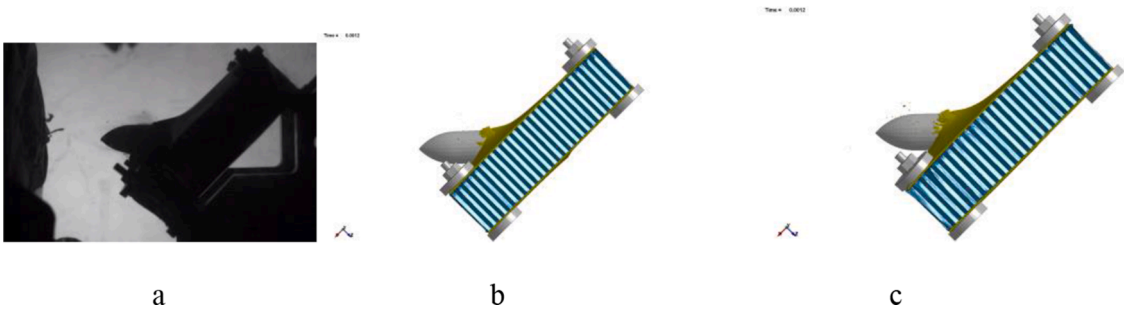

Figure 18. Views of experimental and numerical results for ogive nose oblique impact configuration with projectile penetrating rear sheet. (a) Experimental 94m/s (b) PLP 93 m/s (c) TJC 93 m/s

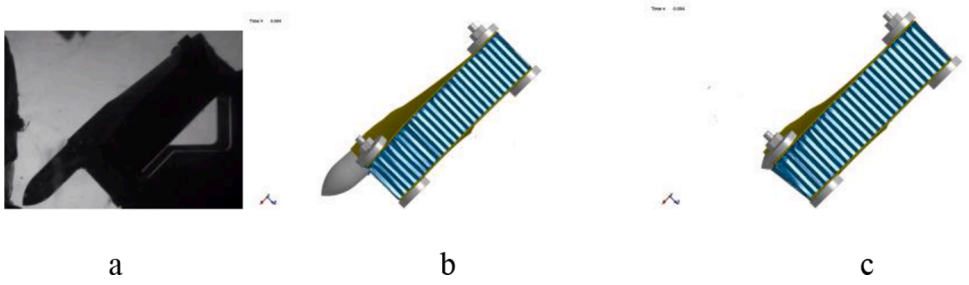

Figure 19. Views of experimental and numerical results for ogive nose oblique impact configuration with projectile deflected by rear sheet. (a) Experimental 59 m/s (b) PLP 55 m/s (c) TJC 55 m/s

honeycomb core, resulting in local crushing of the honeycomb ahead of the projectile. A plug recovered from an experiment is shown in fig. 20. In the numerical results this behaviour is not seen. The numerical model is not capable of capturing this local crushing behaviour due the erosion criterion for failure that allows the projectile to penetrate through the honeycomb, resulting in an overestimate of the exit velocity, fig. 21. While broadly similar behaviour is seen in the numerical and experimental results, fig. 22, the level of deformation and damage in the rear sheet is less in the simulations than in the experiments. Modelling options to capture this honeycomb crushing in the numerical simulations were investigated. It did not prove possible to capture both the crush and penetration behaviour with the detailed shell honeycomb model. The option of using solid elements for the honeycomb does allow the crush and penetration behaviour to be represented together, however the solid element honeycomb model significantly overestimated the energy absorbed by the honeycomb in the oblique and ogive nose impact cases. A single modelling approach that provided acceptable results across the range of impact cases considered was not found.

Figure 20. Plug formed by front sheet and crushed honeycomb, recovered from 90 m/s experiment.

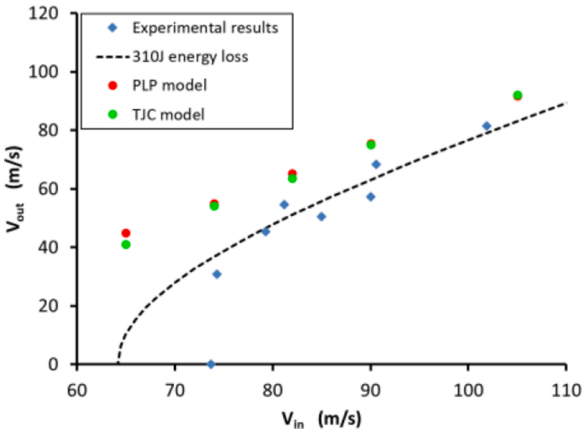

Figure 21. Flat nose normal impact configuration model results plotted with the experimental results and the 310J energy loss fit to the experimental data. The graph shows projectile exit velocity, V_{out}, against initial impact velocity, V_{in}.

4.4. Flat nose oblique impact configuration

For this configuration analyses were run for six impact velocities: 60 m/s, 70 m/s, 80 m/s, 93 m/s, 100 m/s and 113 m/s. These velocities cover the range of impact conditions tested experimentally.

A graph of projectile exit velocity against impact velocity is shown in fig. 23. The numerical results overestimate the projectile exit velocity. Comparison with the experimental high speed video shows overall similar behaviour, fig. 24, showing that the basic mechanics is represented reasonably. Unlike for the flat nose normal impact case no single reason for the overestimate was identified.

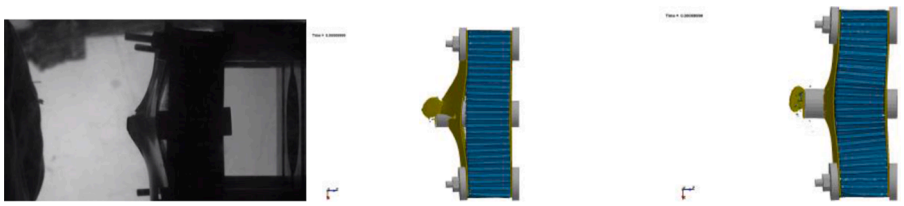

a b c

Figure 22. Views of experimental and numerical results for flat nose normal impact configuration with projectile penetrating rear sheet. (a) Experimental 90m/s (b) PLP 90 m/s (c) TJC 90 m/s

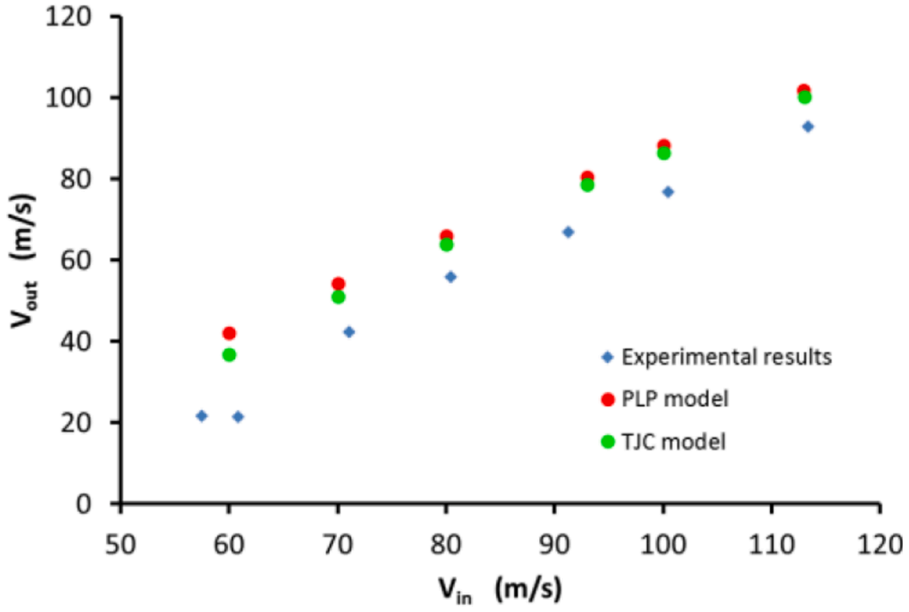

Figure 23. Flat nose oblique impact configuration model results plotted with the experimental results.

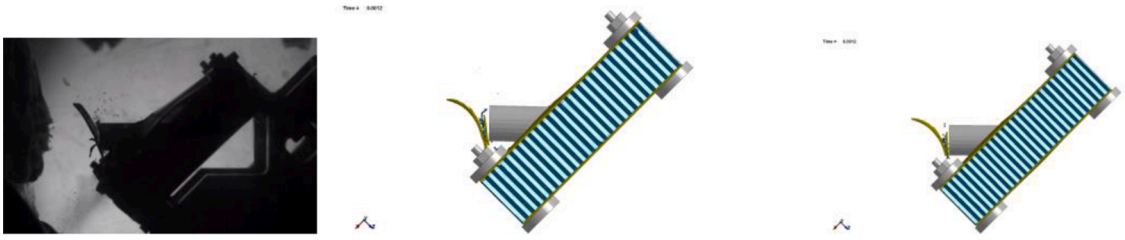

a b c

Figure 24. Views of experimental and numerical results for flat nose oblique impact configuration. (a) Experimental 80m/s (b) PLP 80 m/s (c) TJC 80 m/s

4.5. Mesh Sensitivity

Given the mesh sensitivity observed with the continuum damage mechanics material model it was decided to investigate the mesh sensitivity of the results further. In the face sheet mesh used in the main study, fig. 5, the central elements are approximately cubic with an edge length of 0.25-0.27mm. In this section this model is referred to as the reference model. Three alternative meshes for the face sheets were generated:

- **Uniform** Entire face sheet meshed with cubic elements of uniform size with edge length 0.254mm, fig. 25 a.
- **Unstructured** Face sheet mesh generated with auto meshing tool to remove overall structure and hence preferential mesh directions. Element size similar to reference model, fig. 25 b.
- **Fine** Higher resolution mesh with seven elements through thickness, to match the resolution used in the previous study on modelling the ballistic limit of aluminium plates [3]. The resulting central element edge lengths were 0.18-0.2mm, fig. 25 c.

All three face sheet meshes were combined with a higher resolution honeycomb model with six elements along each cell edge. All other aspects of the models, including material properties, contact algorithms and support mesh are unchanged. Table 3 presents a summary of the models and example run times for the ogive nose normal impact case

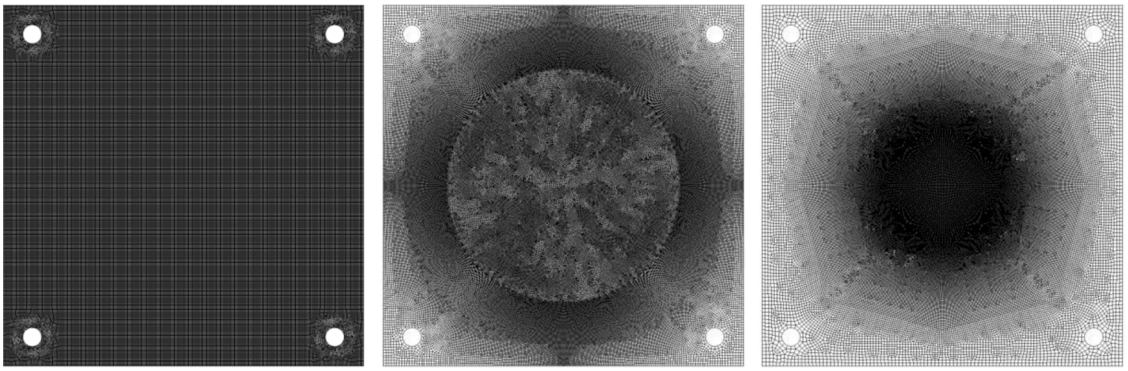

a b c

Figure 25. Face sheet meshes. (a) Uniform (b) Unstructured (c) Fine

Table 3
Summary of mesh sensitivity models. The run times shows are the wall clock times to a solution time.

Model	N solid elements in face sheets	N shell elements in core	Initial element minimum Δt (*ns*)	Initial model Δt (*ns*)	PLP run time† (minutes)	TJC run time† (minutes)
Reference	502,720	378,160	14.97	10.77*	334	274
Uniform	2,374,440	1,890,720	16.69	16.69	656	1435
Unstructured	1,785,240	1,890,720	15.09	9.44*	2737	1117
Fine	1,830,332	1,890,720	10.81	6.00*	1581	3941

* Where the initial model Δt is smaller than the element Δt, the cause is the contact algorithm.
† All times shown are the wall clock time to a solution time of t = 2.4 ms.

running on a 24 core linux node.

All models were run with both the PLP and TJC material models for four impact cases, covering both normal and oblique impact with the ogive nose projectile and normal impact with the flat nose projectile. Projectile exit velocities for all cases are shown in table 4. As the unstructured mesh model proved less robust than the other three models, projectile exit velocities could not be obtained in three runs where analyses terminated due to numerical problems before the projectile fully exited the panel. Figure 26 compares the panel deformation for the ogive nose normal impact case. Both the exit velocity results and overall panel behaviour show that there is some mesh sensitivity present in the model.

For the normal impact cases the uniform panel mesh gives results generally similar to the reference mesh, although with differences in the deformation of the rear sheet that, for the TJC model, visually improve agreement with the behaviour seen in the experimental high-speed videos. This is consistent with the uniform mesh, which avoids high aspect ratio elements near the boundary, improving the overall sheet behaviour. This is particularly apparent in the 55 m/s oblique impact case. The uniform mesh does require a large number of elements, increasing both the runtime and the diskspace requirements for holding the LS-DYNA output files.

The overall behaviour seen with the fine mesh model is similar to the reference model, except for the 55 m/s oblique impact case where the projectile penetrates through the rear sheet. As both element failure models were tuned using the reference mesh, and as neither uses any terms based on element length to reduce sensitivity, it is reasonable that a finer mesh does influence the sheet failure behaviour and hence the projectile exit velocities. The unstructured mesh model also sees the projectile penetrating through the rear sheet in the 55 m/s case. This deflection behaviour is sensitive to the element failure model, as the deflection of the projectile by the front sheet influences the impact conditions for the rear sheet. The unstructured mesh model does have a strong influence on the details of element deletion and so the local response of the sheets around the projectile path.

Table 4
Exit velocities for mesh sensitivity analyses

Model	0° Ogive 74 m/s		45° Ogive 93 m/s		45° Ogive 55 m/s		0°Flat 90 m/s	
	PLP	TJC	PLP	TJC	PLP	TJC	PLP	TJC
Reference	55.8	55.1	75.7	71.9	18.3	0.0	75.5	75.1
Uniform	55.0	55.1	75.0	70.4	26.3	21.0	77.3	73.8
Unstructured	57.1	54.2	76.9	73.1	17.1*	-	-	-
Fine	57.4	57.7	78.1	76.6	23.5*	17.4*	76.5	75.7

* projectile penetrates rear sheet, it is not deflected.

4.6. Modelling tool

The modelling approach selected for the design tool combined the reference mesh model with the PLP material model. This combination has demonstrated the ability to predict the projectile residual velocity and ballistic limit under normal and oblique impact conditions, particularly for the ogive nose case. This represents the primary requirement for the tool. The reference model minimises the computational resources required for analysis, important as harpoon impact involves larger target panel structures. While including influences such as strain-rate and stress triaxiality delivered improved visual agreement for panel deformation, significant assumptions have been made in defining the material properties used. Consequently further model development, supported by additional experimental material characterisation, is required to use this.

5. Conclusions

In this paper a modelling tool is developed for harpoon design for active orbital debris removal. The tool is capable of predicting the ballistic limit of an aluminium sandwich panel representative of a large satellite structural element, and its sensitivity to variation in impact conditions. The modelling method is based on the use of a detailed explicit finite element model for the panel, with an element failure criterion used to approximate material damage and failure. In developing the model, sensitivity studies were used to investigate the influence of

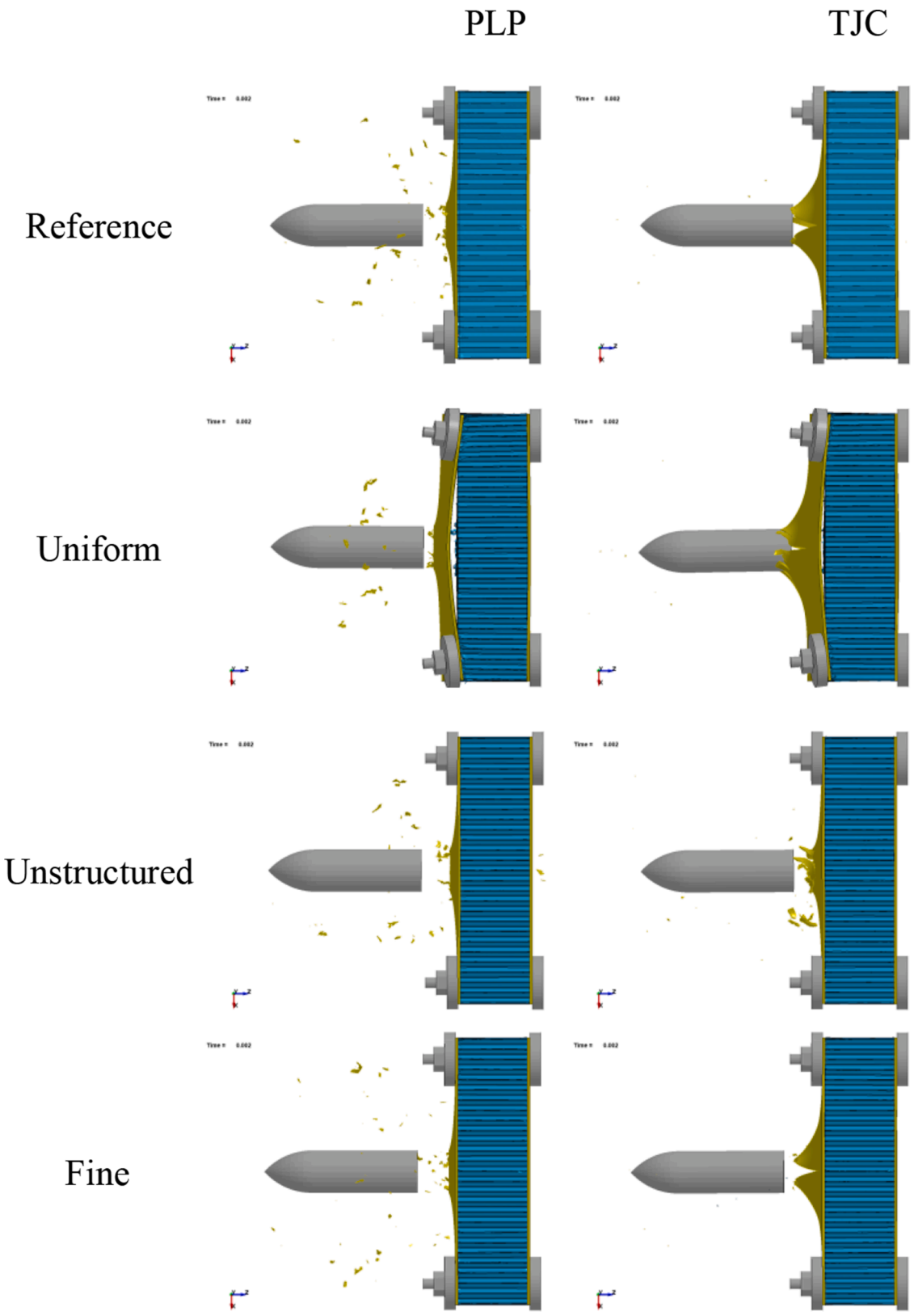

Figure 26. Numerical results for the four different meshes and two material models. All results are for a solution time of t = 2.0 ms and an initial projectile velocity of 74 m/s.

model features on the projectile exit velocity, for a specific impact case. Information from these studies was then used to generate the final model.

The modelling method was tested for both normal and oblique impact of ogive and flat nose projectiles on the panel. The main conclusions from these analyses were:

- For the ogive nose projectile, the exit velocity agreed well with the experiments for the range of impact velocities and angles considered.
- For the flat nose projectile, the model overestimated the exit velocity. In the case of the normal impact this was due to the model not representing the honeycomb crush ahead of the projectile.
- The model features with the most significant influence on the projectile exit velocity are the face sheet material modelling and the projectile-panel friction model. In the final model both features required assumptions that were tuned against exit velocity for a single impact condition. Improving either assumption would require more extensive experimental testing than was possible in this study.
- The use of an element deletion criterion that incorporated the influence of stress triaxiality improved the agreement for the plate deformation behaviour between the numerical and experimental results.
- An investigation of mesh sensitivity showed that mesh size and design did have an influence on the results, and that parameters such as element erosion that do introduce mesh sensitivity into the model have to be verified for the specific mesh used.

The modelling approach selected for the design tool combined the reference mesh model with the simpler material model. The numerical results demonstrated that this combination delivered the primary requirement for the tool, the ability to predict the ballistic limit under a range of impact conditions.

CRediT authorship contribution statement

J.C. Campbell: Conceptualization, Methodology, Investigation, Writing – original draft. **K. Hughes:** Methodology, Validation. **R. Vignjevic:** Conceptualization, Writing – review & editing. **N. Djordjevic:** Methodology, Writing – review & editing. **N. Taylor:** Investigation. **A. Jardine:** Investigation, Writing – review & editing.

Declaration of Competing interest

The authors declare that they have no known competing financial interests or personal relationships that could have appeared to influence the work reported in this paper.

Acknowledgements

The experimental tests and part of the modelling work were funded by the European Space Agency under a contract with Airbus Defence and Space.

References

[1] Orbital Debris Quarterly News. Volume 25, Issue 1. NASA Orbital Debris Program Office. February 2021.
[2] Liou J-C, Johnson NL, Hill NM. Controlling the growth of future LEO debris populations with active debris removal. Acta Astronaut 2010;66:648. https://doi.org/10.1016/j.actaastro.2009.08.005.
[3] Vuyst TD, Vignjevic R, Albero AA, Hughes K, Campbell JC, Djordjevic N. The effect of the orientation of cubical projectiles on the ballistic limit and failure mode of AA2024-T351 sheets. Int J Impact Eng 2017;104:21–37. https://doi.org/10.1016/j.ijimpeng.2017.01.026.
[4] Lin C, Fatt MSH. Perforation of Composite Plates and Sandwich Panels under Quasi-static and Projectile Loading. J Compos Mater 2006;40:1801. https://doi.org/10.1177/0021998306060173.
[5] Hou W, Zhu F, Lu G, Fang D-N. Ballistic impact experiments of metallic sandwich panels with aluminium foam core. Int J Impact Eng 2010;37:1045. https://doi.org/10.1016/j.ijimpeng.2010.03.006.
[6] Yungwirth CJ, Radford DD, Aronson M, Wadley HNG. Experiment assessment of the ballistic response of composite pyramidal lattice truss structures. Compos Part B Eng 2008;39:556. https://doi.org/10.1016/j.compositesb.2007.02.029.
[7] Fatt MSH, Park KS. Perforation of honeycomb sandwich plates by projectiles. Compos Part Appl Sci Manuf 2000;31:889. https://doi.org/10.1016/s1359-835x(00)00021-x.
[8] Goldsmith W, Wang G-T, Kezhun L, Crane D. Perforation of cellular sandwich plates. Int J Impact Eng 1997;19:361. https://doi.org/10.1016/s0734-743x(97)00003-1.
[9] Kolopp A, Alvarado RA, Rivallant S, Bouvet C. Modeling impact on aluminium sandwich including velocity effects in honeycomb core. J Sandw Struct Mater 2013;15:733. https://doi.org/10.1177/1099636213501102.
[10] Kolopp A, Rivallant S, Bouvet C. Experimental study of sandwich structures as armour against medium-velocity impacts. Int J Impact Eng 2013;61:24–35. https://doi.org/10.1016/j.ijimpeng.2013.05.007.
[11] Sun G, Chen D, Wang H, Hazell PJ, Li Q. High-velocity impact behaviour of aluminium honeycomb sandwich panels with different structural configurations. Int J Impact Eng 2018;122:119. https://doi.org/10.1016/j.ijimpeng.2018.08.007.
[12] Rahimijonoush A, Bayat M. Experimental and numerical studies on the ballistic impact response of titanium sandwich panels with different facesheets thickness ratios. Thin Wall Struct 2020;157:107079. https://doi.org/10.1016/j.tws.2020.107079.
[13] Avallone EA, Baumeister T. Marks' Standard Handbook for Mechanical Engineers. 10th ed. McGraw-Hill; 1996.
[14] Recht RF. High Velocity Impact Dynamics: Analytical Modeling of Plate Penetration Dynamics. editor. In: Zukas JA, editor. High Velocity Impact Dynamics. John Wiley & Sons; 1990.
[15] Hartley RS, Cloete TJ, Nurick GN. An experimental assessment of friction effects in the split Hopkinson pressure bar using the ring compression test. Int J Impact Eng 2007;34:1705–28. https://doi.org/10.1016/j.ijimpeng.2006.09.003.
[16] Philippon S, Sutter G, Molinari A. An experimental study of friction at high sliding velocities. Wear 2004;257:777–84. https://doi.org/10.1016/j.wear.2004.03.017.
[17] Aluminum Standards and Data. The Aluminium Association Inc.; 1996.
[18] HexWeb^{TM} Honeycomb Attributes and Properties. Hexcel Composites; 1999.
[19] LSTC Offset Deformable Barrier Models v2.0.1. Livermore Software Technology Corporation (LSTC); 2014.
[20] LS-DYNA R10. 0 Keyword User's Manual. Livermore, USA: Livermore Software Technology Corporation (LSTC); 2017.
[21] Dufailly J, Lemaitre J. Modeling Very Low Cycle Fatigue. Int J Damage Mech 1995;4:153–70. https://doi.org/10.1177/105678959500400204.
[22] Belytschko T, Liu WK, Moran B. Nonlinear finite elements for continua and structures. John Wiley & Sons; 2000.
[23] Johnson GR, Cook WH. Fracture characteristics of three metals subjected to various strains, strain rates, temperatures and pressures. Eng Fract Mech 1985;21:31–48. https://doi.org/10.1016/0013-7944(85)90052-9.
[24] Gupta NK, Iqbal MA, Sekhon GS. Experimental and numerical studies on the behavior of thin aluminum plates subjected to impact by blunt- and hemispherical-nosed projectiles. Int J Impact Eng 2006;32:1921. https://doi.org/10.1016/j.ijimpeng.2005.06.007.
[25] Asad M, Girardin F, Mabrouki T, Rigal J-F. Dry cutting study of an aluminium alloy (A2024-T351): a numerical and experimental approach. Int J Mater Form 2008;1:499. https://doi.org/10.1007/s12289-008-0150-9.
[26] Iqbal MA, Gupta PK, Deore VS, Tak SK, Tiwari G, Gupta NK. Effect of target span and configuration on the ballistic limit. Int J Impact Eng 2012;42:11. https://doi.org/10.1016/j.ijimpeng.2011.10.004.
[27] Iqbal MA, Senthil K, Bhargava P, Gupta NK. The characterization and ballistic evaluation of mild steel. Int J Impact Eng 2015;78:98–113. https://doi.org/10.1016/j.ijimpeng.2014.12.006.
[28] Vershinin VV. Validation of metal plasticity and fracture models through numerical simulation of high velocity perforation. Int J Solids Struct 2015;67:127–38. https://doi.org/10.1016/j.ijsolstr.2015.04.007.
[29] Antoinat L, Kubler R, Barou J-L, Viot P, Barrallier L. Perforation of aluminium alloy thin plates. Int J Impact Eng 2015;75:255. https://doi.org/10.1016/j.ijimpeng.2014.07.017.
[30] Wang Y, Chen X, Xiao X, Vershinin VV, Ge R, Li D. Effect of Lode angle incorporation into a fracture criterion in predicting the ballistic resistance of 2024-T351 aluminum alloy plates struck by cylindrical projectiles with different nose shapes. Int J Impact Eng 2020;139:103498. https://doi.org/10.1016/j.ijimpeng.2019.103498.
[31] Johnson GR, Cook WH. A constitutive model and data for metals subjected to large strains, high strain rates and high temperatures. In: Proceedings of the 7th International Symposium on Ballistics. Netherlands: The Hague; 19-23 April 1983. p. 541–7.
[32] Leuser D. Experimental Investigations of Material Models for Ti-6AL-4V and 2024-T3. Lawrence Livermore National Laboratory; 1999.
[33] Wierzbicki T, Bao Y, Lee Y-W, Bai Y. Calibration and evaluation of seven fracture models. Int J Mech Sci 2005;47:719–43. https://doi.org/10.1016/j.ijmecsci.2005.03.003.